AD-A132 341 CHARACTERIZATION OF THE STRUCTURE AND SUBSTRUCTURE OF THERMALLY TRANSFORM..(U) NAVAL POSTGRADUATE SCHOOL MONTEREY CA P W BOBOWIEC JUN 83 1/1

UNCLASSIFIED F/G 11/6 NL

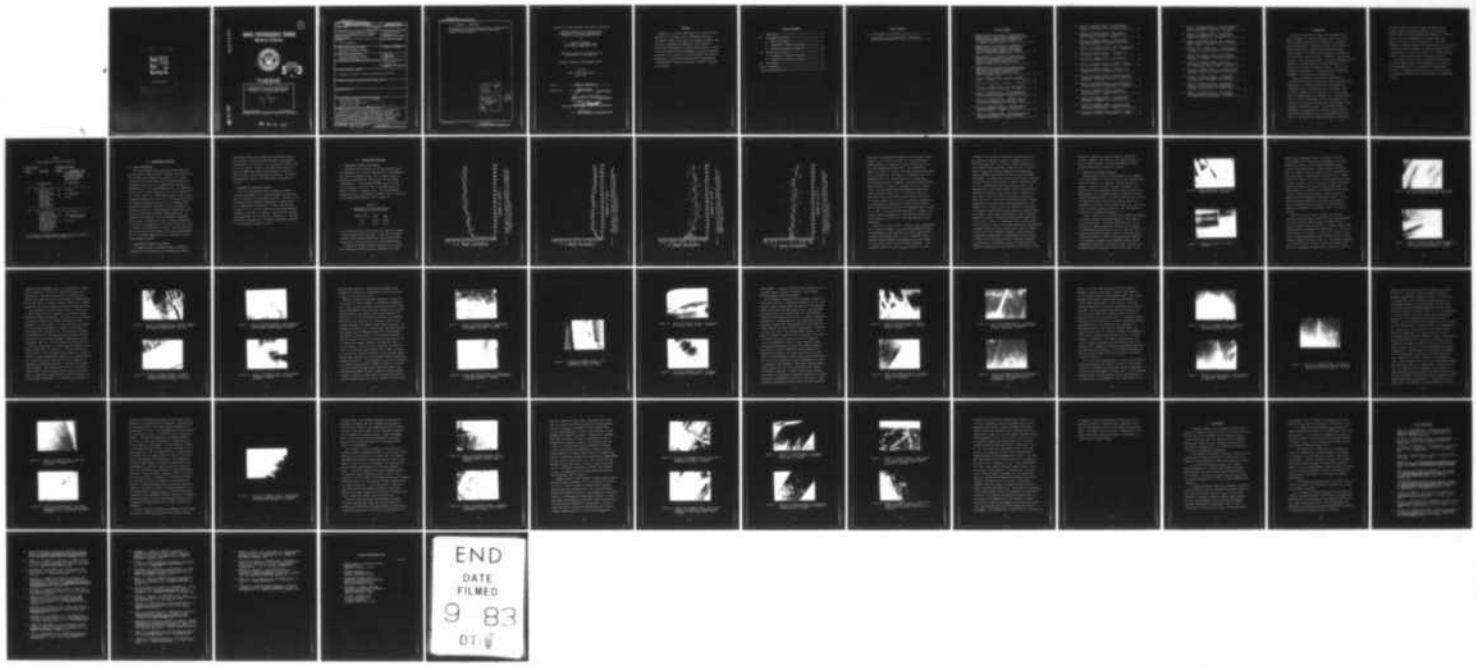

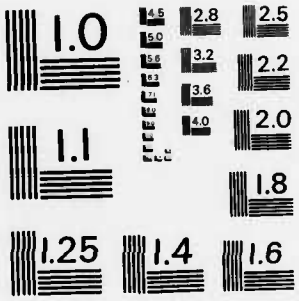

MICROCOPY RESOLUTION TEST CHART
NATIONAL BUREAU OF STANDARDS-1963-A

AD A132341

(2)

NAVAL POSTGRADUATE SCHOOL

Monterey, California

DTIC
ELECTE
SEP 9 1983
S D
B

THESIS

CHARACTERIZATION OF THE STRUCTURE AND SUBSTRUCTURE OF THERMALLY TRANSFORMATION CYCLED Cu-Zn-Al SHAPE MEMORY ALLOYS

by

Paul W. Bobowiec

June 1983

Thesis Advisor: J. Perkins

Approved for public release; distribution unlimited.

DTIC FILE COPY

83 09 07 168

UNCLASSIFIED

SECURITY CLASSIFICATION OF THIS PAGE (When Data Entered)

REPORT DOCUMENTATION PAGE		READ INSTRUCTIONS BEFORE COMPLETING FORM
1. REPORT NUMBER	2. GOVT ACCESSION NO. AD-A132341	3. RECIPIENT'S CATALOG NUMBER
4. TITLE (and Subtitle) Characterization of the Structure and Substructure of Thermally Transformation Cycled Cu-Zn-Al Shape Memory Alloys		5. TYPE OF REPORT & PERIOD COVERED Master's Thesis; June 1983
		6. PERFORMING ORG. REPORT NUMBER
7. AUTHOR(s) Paul W. Bobowiec		8. CONTRACT OR GRANT NUMBER(s)
9. PERFORMING ORGANIZATION NAME AND ADDRESS Naval Postgraduate School Monterey, California 93940		10. PROGRAM ELEMENT, PROJECT, TASK AREA & WORK UNIT NUMBERS
11. CONTROLLING OFFICE NAME AND ADDRESS Naval Postgraduate School Monterey, California 93940		12. REPORT DATE June 1983
		13. NUMBER OF PAGES 57
14. MONITORING AGENCY NAME & ADDRESS(if different from Controlling Office)		15. SECURITY CLASS. (of this report) Unclassified
		15a. DECLASSIFICATION/DOWNGRADING SCHEDULE

16. DISTRIBUTION STATEMENT (of this Report)

Approved for public release; distribution unlimited

17. DISTRIBUTION STATEMENT (of the abstract entered in Block 20, if different from Report)

18. SUPPLEMENTARY NOTES

19. KEY WORDS (Continue on reverse side if necessary and identify by block number)

Shape Memory Effect Cu-Zn-Al

Martensitic Transformation

Copper Base Alloys (Copper-Zinc-Aluminum)

20. ABSTRACT (Continue on reverse side if necessary and identify by block number)

Samples of a Cu-Zn-Al shape memory alloy were thermally cycled up to 100 times, using a differential scanning calorimeter, between the parent and martensite phases. The trends of transformation temperature versus number of cycles were correlated with observed microstructure. Specimens were examined through transmission electron microscopy techniques. The character of lattice defects and residual

DD FORM 1 JAN 73 1473 EDITION OF 1 NOV 65 IS OBSOLETE

S/N 0102-LF-014-6601

UNCLASSIFIED

SECURITY CLASSIFICATION OF THIS PAGE (When Data Entered)

20 - ABSTRACT - (CONTINUED)

structures in the parent phase provided an understanding of substructural conditions enhancing martensite formation and reversion.

Accession For	
NTIS GRA&I	☑
DTIC TAB	☐
Unannounced	☐
Justification	
By	
Distribution/	
Availability Codes	
Dist	Avail and/or Special
A	

DTIC COPY INSPECTED 2

Approved for public release; distribution unlimited.

Characterization of the Structure and Substructure of Thermally Transformation Cycled Cu-Zn-Al Shape Memory Alloys

by

Paul W. Bobowiec
Lieutenant, United States Navy
B.A., Boston University, 1974

Submitted in partial fulfillment of the requirements for the degree of

MASTER OF SCIENCE IN ENGINEERING SCIENCE

from the

NAVAL POSTGRADUATE SCHOOL
June 1983

Author: Paul W. Bobowiec

Approved by: Jeff Perkins
Thesis Advisor

Kenneth D. Challenger
Second Reader

P. J. Marto
Chairman, Department of Mechanical Engineering

J. N. Dyer
Dean of Science and Engineering

ABSTRACT

Samples of a Cu-Zn-Al shape memory alloy were thermally cycled up to 100 times, using a differential scanning calorimeter, between the parent and martensite phases. The trends of transformation temperature versus number of cycles were correlated with observed microstructure. Specimens were examined through transmission electron microscopy techniques. The character of lattice defects and residual structures in the parent phase provided an understanding of substructural conditions enhancing martensite formation and reversion.

TABLE OF CONTENTS

I. INTRODUCTION ---------- 10

II. EXPERIMENTAL PROCEDURE ---------- 13

A. SAMPLE PREPARATION ---------- 13

B. DIFFERENTIAL SCANNING CALORIMETRY ---------- 13

C. TRANSMISSION ELECTRON MICROSCOPY ---------- 14

III. RESULTS AND DISCUSSION ---------- 15

A. DIFFERENTIAL SCANNING CALORIMETRY ---------- 15

B. TRANSMISSION ELECTRON MICROSCOPY ---------- 22

IV. CONCLUSIONS ---------- 51

LIST OF REFERENCES ---------- 53

INITIAL DISTRIBUTION LIST ---------- 57

LIST OF TABLES

I. Phase Symbols and Structure Notation ---------- 12

II. Temperature (K) of Maximum Rate of Transformation for First Cycle ---------- 15

LIST OF FIGURES

1. Sample group D-1's variation of temperature of maximum rate of parent phase to martensite transformation minus temperature of maximum rate of transformation during first thermal cycle vs. number of thermal cycles ---------- 16

2. Sample group D-2's variation of temperature of maximum rate of parent phase to martensite transformation minus temperature of maximum rate of transformation during first thermal cycle vs. number of thermal cycles ---------- 17

3. Sample group D-1's variation of temperature of maximum rate of martensite reversion to parent phase minus temperature of maximum rate of reversion during first thermal cycle vs. number of thermal cycles ---------- 18

4. Sample group D-2's variation of temperature of maximum rate of martensite reversion to parent phase minus temperature of maximum rate of reversion during first thermal cycle vs. number of thermal cycles ---------- 19

5. Alloy F showing internally twinned martensite plates. (40,000X) ---------- 23

6. Close up of interface of Figure 5. (200,000X) ---- 23

7. Alloy D (1 thermal cycle). The light traces of vestigial ridges are evident. (27,000X) ------- 25

8. Alloy D (1 thermal cycle). Self-accommodating plates are seen with perpendicular needle-like stress-induced martensite. (14,000X) ---------- 25

9. Alloy D (5 thermal cycles). Numerous vestigial variants are displayed including fork, spear and butterfly morphologies. (10,000X) ---------- 27

10. Alloy D (5 thermal cycles). A residual martensite plate exhibits internally twinned and banded structure. (5,000X) ---------- 27

11. Alloy D (5 thermal cycles). The intersection of three grains reveals different vestige-grain boundary relationships. (5,000X) ---------- 28

12. Alloy D (5 thermal cycles). With increased cycling, the surface relief of ridges increase. (5,000X) ---------- 28

13. Alloy D (10 thermal cycles). Two distinct orientations of the vestigial ridges to the grain boundary are shown. (10,000X) ---------- 30

14. Alloy D (10 thermal cycles). A magnification of the spear structure of Figure 13 reveals a step-type structure. (27,000X) ---------- 30

15. Alloy D (10 thermal cycles). Self-accommodating nature of plate structure is shown. (27,000X) ---- 31

16. Alloy D (10 thermal cycles). An area with one residual plate is shown. (27,000X) ---------- 32

17. Alloy D (10 thermal cycles). A close-up of the plate of Figure 16. (10,000X) ---------- 32

18. Alloy D (10 thermal cycles). Another residual plate is bounded by a mottled matrix. (14,000X) -- 34

19. Alloy D (10 thermal cycles). A close-up view of the plate-matrix interface of Figure 18. (40,000X) ---------- 34

20. Alloy D (15 thermal cycles). Dislocations have a distinct angular relationship with vestigial structures. (20,000X) ---------- 35

21. Alloy D (15 thermal cycles). A continuation of Figure 20 shows the concentration of dislocations to a distinct region of the matrix. (20,000X) ---- 35

22. Alloy D (15 thermal cycles). Dislocation structures are seen in relationship to two grain boundaries. (14,000X) ---------- 37

23. Alloy D (15 thermal cycles). The equidistant and band-type segregation of dislocations is displayed. (20,000X) ---------- 37

24. Alloy D (15 thermal cycles). As cycling continues, the surface relief of vestigial ridges continues to be enhanced. (14,000X) ---------- 38

25. Alloy D (15 thermal cycles). Vestigial ridges are shown in a parallel arrangement. (14,000X) --- 40

26. Alloy D (15 thermal cycles). At higher magnification, a vestigial ridge of Figure 25 shows a distinct martensitic structure. (100,000X) ------- 40

27. Alloy D (15 thermal cycles). Parallelpiped reliefs are possible vestigial structures of diamond-type martensite. (10,000X) ---------- 42

28. Alloy D (100 thermal cycles). With increasing number of cycles, the interaction of vestigial forms is shown. (10,000X) ---------- 44

29. Alloy D (100 thermal cycles). On magnification of Figure 28, a γ-type structure is revealed. (27,000X) ---------- 44

30. Alloy D (100 thermal cycles). With further cycling, the formation of butterfly martensite increases. (14,000X) ---------- 46

31. Alloy D (100 thermal cycles). The severe interaction of plates is revealed by the growth of a double spear within a fork. (14,000X) ------- 46

32. Alloy D (77 thermal cycles). A distinct contour of lattice defects is contained in the plate. (20,000X) ---------- 47

33. Alloy D (77 thermal cycles). A continuation of Figure 32 exhibits banded and displaced stacking faults. (20,000X) ---------- 47

34. Alloy D (77 thermal cycles). The stacking faults of Figure 33 have been displaced by an internal twinning action of the martensite. (40,000X) ---------- 48

35. Alloy D (77 thermal cycles). The stacking faults contained in the contour of Figure 32 are displayed in magnification. (200,000X) ------- 48

I. INTRODUCTION

Martensite structures and mode of transformation have been the objects of continual research, partly due to the direct practical applications of theoretical and experimental observations. Shape memory alloys, whose useful and unique properties are governed by martensitic behavior characteristics, are currently being applied as metallurgical solutions to varied electrical, mechanical, and surgical problems. Olson and Hartman [Ref. 1] recently proposed that the martensitic transformation acts as the mechanism for life functions in primitive biological systems. With each new explanation and solution, a different facet of martensitic phenomena is revealed to be in need of study.

During a thermoelastic martensitic transformation, martensite forms from the parent phase below a definite start temperature, M_s, growing continuously with lowering of temperature until a finish point, M_f, is achieved. With increase of temperature, a reversion to the parent phase begins at temperature A_s and ceases at A_f. A unique characteristic of the transformation is that the formation and reversion are along the same paths and is reproducible with subsequent temperature changes. The cooling process is analogous to an application of external stress serving to assist the transformation since, as discussed by Perkins [Ref. 2], the impetus for the transformation is supplied by

a balance between the driving force (the chemical free energy difference between the phases) and the opposing elastic strain energy developed by the formation of the new phase. One of the commercially-viable materials that exhibits this trait is the Cu-Zn-Al alloy. The phase symbology, structure notation and characteristics of the matrix β phase and possible resultant martensitic phases, derived from research by Delaey et al. [Ref. 3] and Dunne and Kennon [Ref. 4], used in this study is summarized in Table I.

The purpose of this study is to examine the effects of multiple thermal cycling on the temperature of maximum rate of transformation and on the resultant microstructural features. The observed phenomenon are intended to provide an increased understanding of the martensitic transformation process.

TABLE I

Phase Symbols and Structure Notation

Matrix Phase		Martensitic Phase	
Symbol	Structure	Symbol	Structure (and stacking with x and x' distinguishing different ordered arrays of atoms in these planes)
β	A2 (bcc disordered)	β'	9R (ABCBCACAB)
β_2	B2 (ordered bcc-CsCl or β_1 Cu-Zn type comprising one cell with copper atom at cell corner sites and solute atom at cell center)	α_2'	3R (ABC)
		β_2'	9R (ABCBCACAB)
		γ_2'	2H (AB)
β_1	DO_3 (ordered bcc-Fe_3Al type consisting of eight cells with copper atoms at all corner sites and at center sites of four cells, and solute atoms at other four center sites)	α_1'	6R (AB'CA'BC')
		β_1'	18R (AB'CB'CA'CA'BA' BC'BC'AC'AB')
		γ_1'	2H (AB')

All martensitic phase structures except β' can be modified (M) or normal (N), depending on composition.

II. EXPERIMENTAL PROCEDURE

A. SAMPLE PREPARATION

The alloys examined were supplied by Delta Metals Research Limited, Ipswich, Suffolk, England. The majority of the research was conducted with samples of 66.2 atomic percent Cu--24.8 atomic percent Zn--9 atomic percent Al, designated as Alloy D with a subambient M_s, derived by Sponholtz [Ref. 5] as approximately 268 K. For comparison, samples of 69.6 atomic percent Cu--14.2 atomic percent Zn--16.1 atomic percent Al, designated as Alloy F, with a M_s as derived by Delaey et al. [Ref. 6], of 350 K were utilized. The materials received as bars of 1.27 cm diameter were quartered and machined into rods of 0.29 cm diameter to facilitate mounting in the TEM specimen holder without the need for electrolytic blanking or spark machining. To homogenize the specimens, they were sealed in evacuated quartz tubes (to prevent zinc loss), solution treated for 15 minutes at a temperature of 1173 K for Alloy D and 1073 K for Alloy F, and quenched in ice water. The rods were then cut into 0.254 mm-thick sections using a low speed diamond saw. All further remarks will be in reference to Alloy D unless otherwise stated.

B. DIFFERENTIAL SCANNING CALORIMETRY

To thermally cycle the specimens and to record the temperatures of the maximum phase transformation rates a

Perkin-Elmer Model DSC-2 Differential Scanning Calorimeter was utilized. Discs were cycled from one to one hundred times between 300 K and 230 K, at a heating and cooling rate of 10 K per minute. Three to five discs were cycled as a group to enhance DSC sensitivity and ensure at least one good thin foil could be obtained from each run. Two groups of samples were cycled one hundred times, designated D-1 and D-2.

C. TRANSMISSION ELECTRON MICROSCOPY

Thin foils were prepared with a Streuers Polipower rectifier and TENUPOL unit, from the thermally cycled discs, using a 3% perchloric acid/methanol solution. The best foils were obtained with solution temperatures of approximately 240 K, pump speed flow rates of 9.5 units, and rectifier voltages of 70 to 75 volts, resulting in rectifier amperage readings of less than .19 amperes. The foils were examined and photographed with the JEOL Ltd., JEM-100 CX II, Electron Microscope, equipped with a Side Entry Goniometer, operated at an accelerating voltage of 100 kV.

III. RESULTS AND DISCUSSION

A. DIFFERENTIAL SCANNING CALORIMETRY

For sample groups thermally cycled one hundred times, the temperatures at which the maximum rate of transformation occurred were recorded as M_{max}, for the parent phase to martensite transformation, and as A_{max}, for the reverse transformation. The difference between M_{max} for a given cycle and M_{max} of the first cycle is plotted versus the number of cycles in Figures 1 and 2. The corresponding variations in A_{max} are plotted in Figures 3 and 4. The first cycle temperature values are given in Table II.

TABLE II

Temperature (K) of Maximum Rate of Transformation for First Cycle

Sample Group	M_{max}	A_{max}
D-1	256.5	280.0
D-2	255.2	273.4

As the ordinate values for the first few cycles are discontinuous from the rest of the data, third order polynomial curve-fits were applied separately to data points representing one to five cycles and six to one hundred cycles.

Although the overall trends of Figures 1 to 4 are the main subject of interest, possible explanations for the

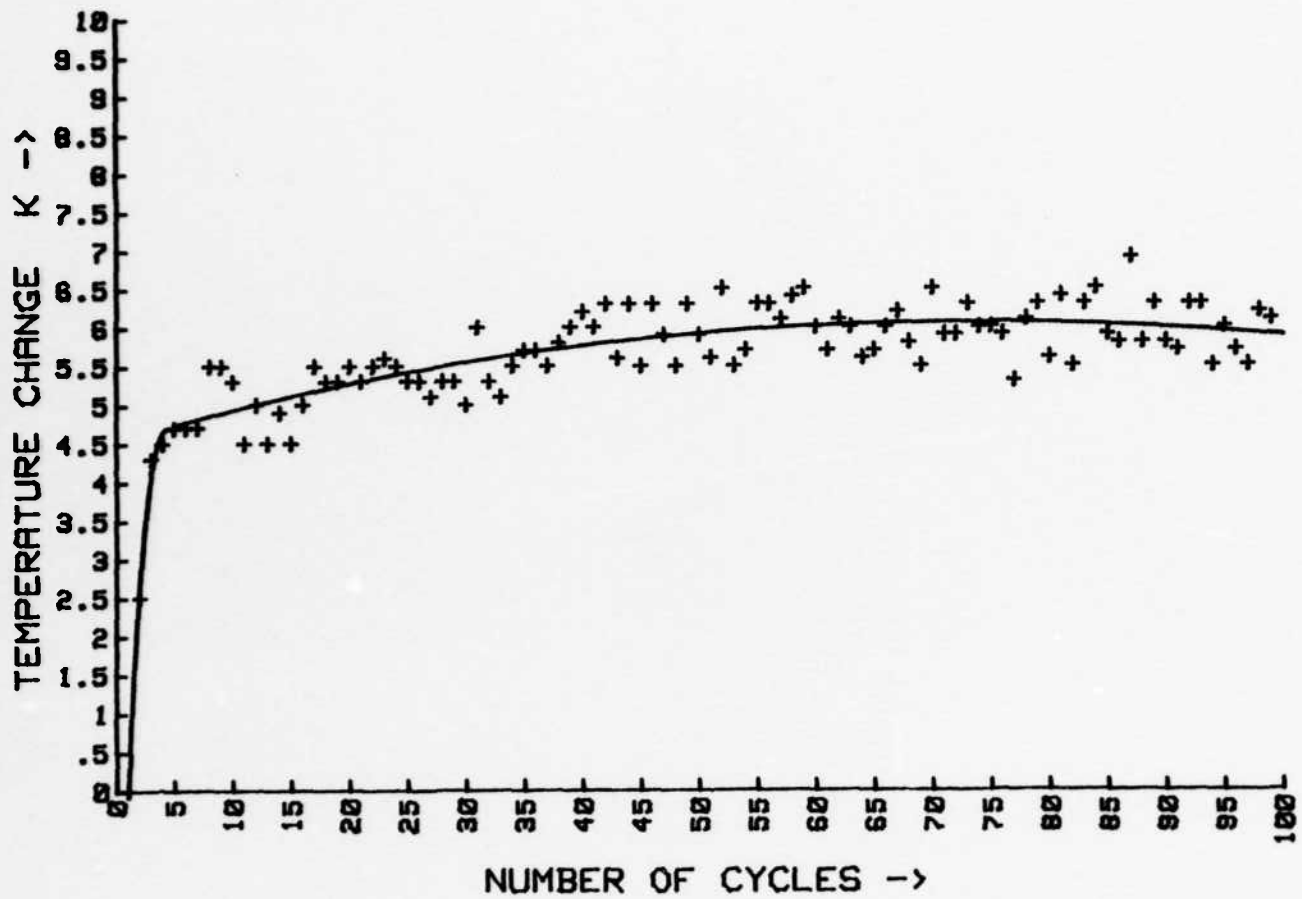

Figure 1. Sample group D-1's variation of temperature of maximum rate of parent phase to martensite transformation minus temperature of maximum rate of transformation during first thermal cycle vs. number of thermal cycles.

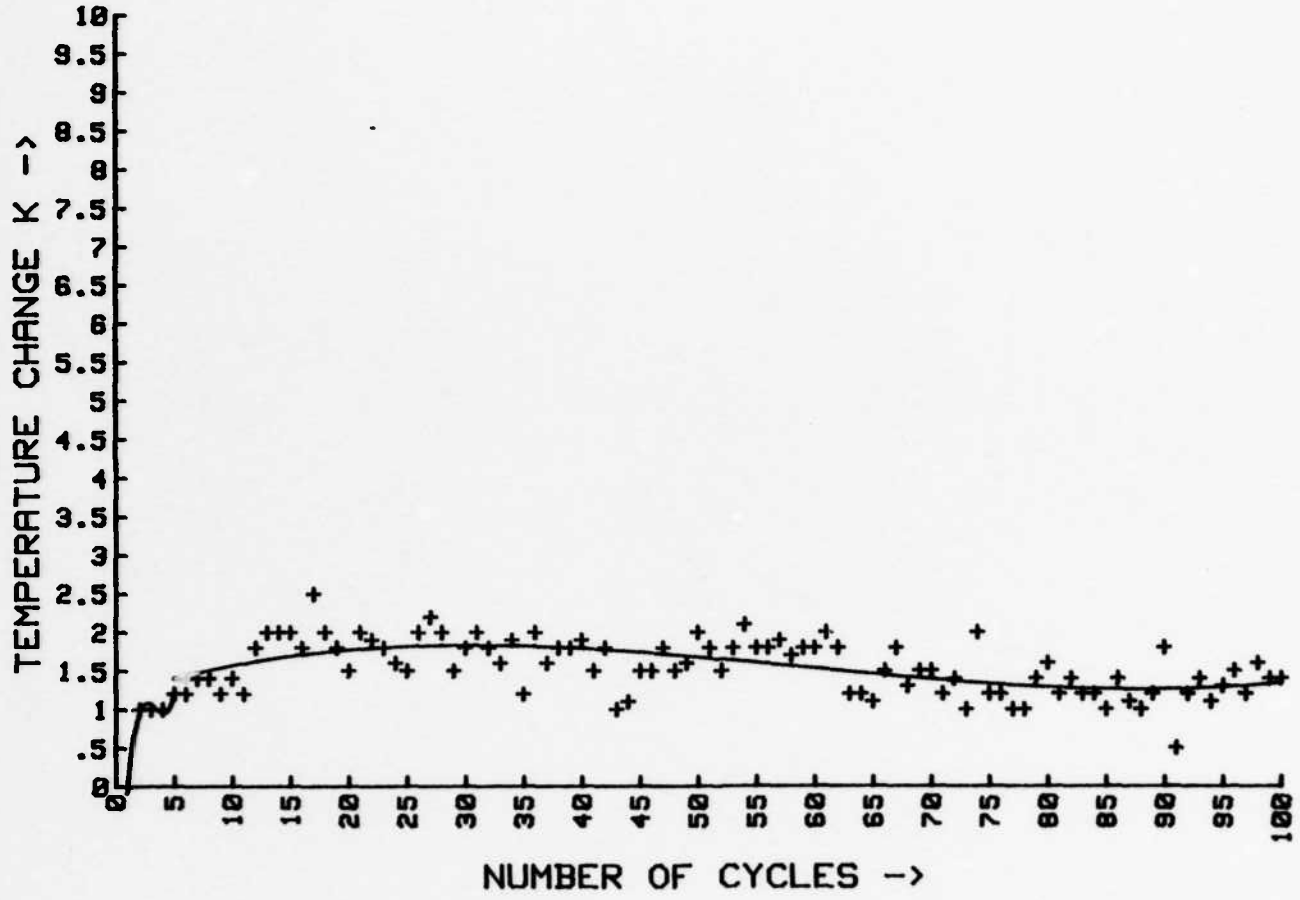

Figure 2. Sample group D-2's variation of temperature of maximum rate of parent phase to martensite transformation minus temperature of maximum rate of transformation during first thermal cycle vs. number of thermal cycles.

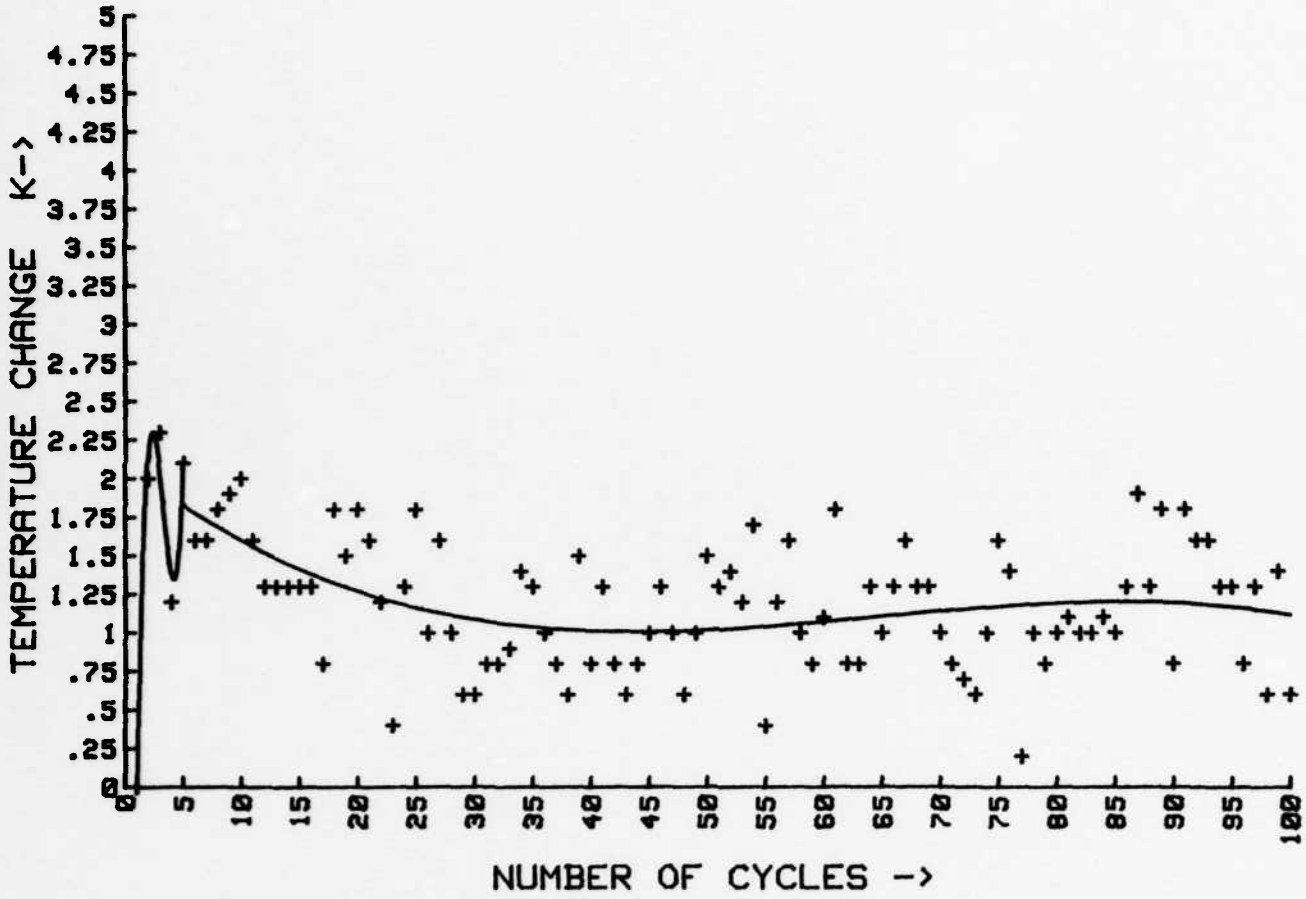

Figure 3. Sample group D-1's variation of temperature of maximum rate of martensite reversion to parent phase minus temperature of maximum rate of reversion during first thermal cycle vs. number of thermal cycles.

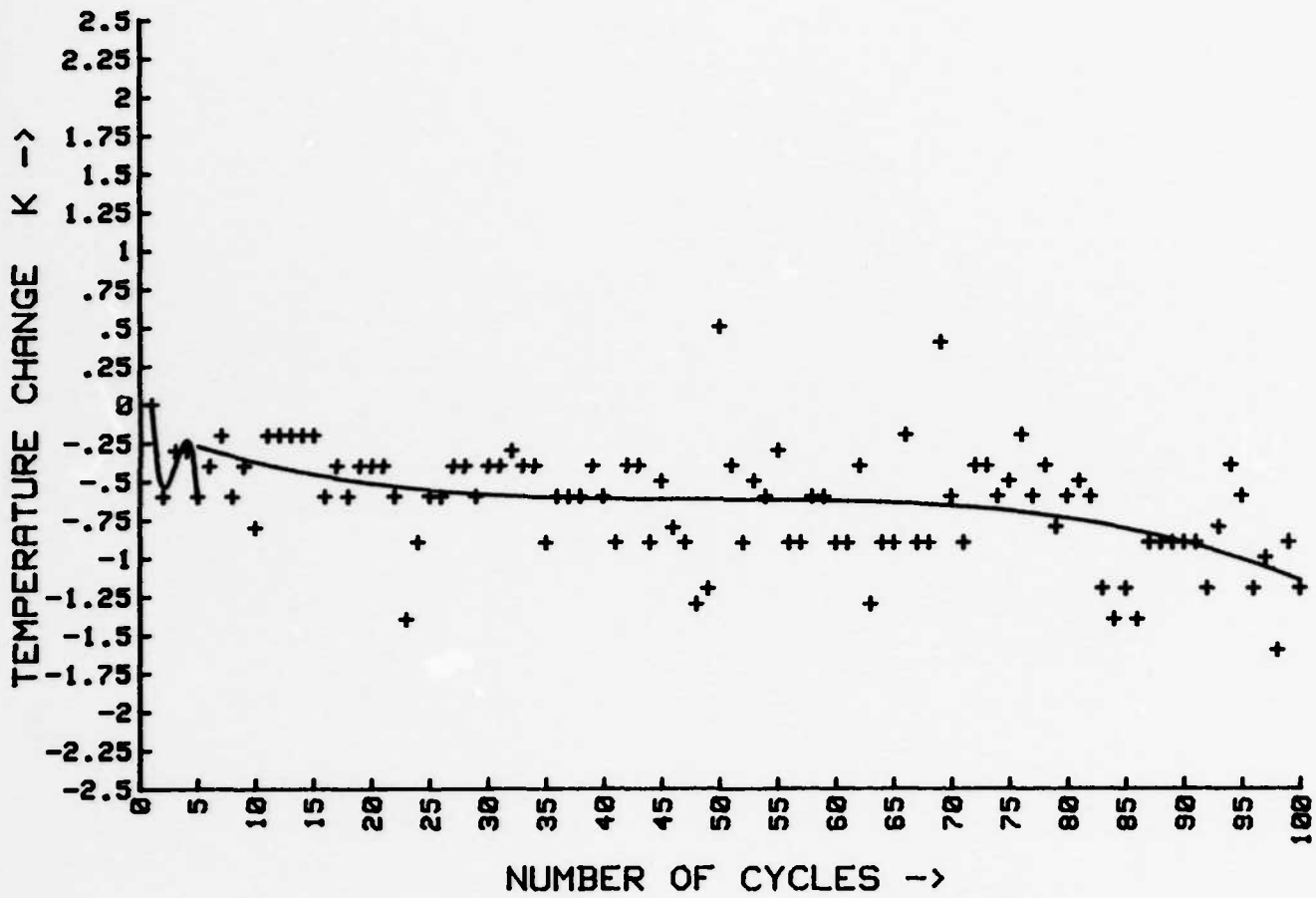

Figure 4. Sample group D-2's variation of temperature of maximum rate of martensite reversion to parent phase minus temperature of maximum rate of reversion during first thermal cycle vs. number of thermal cycles.

difference in corresponding temperature values between sample groups D-1 and D-2 are variations in i) zinc loss during homogenization, ii) recording of initial thermal cycle, or iii) room temperature aging effects. As calculated by Delaey et al. [Ref. 7] a loss of one weight percent zinc raises the M_s by about 22 K. The loss of 0.05 percent zinc in the homogenization of D-1 could account for its higher M_{max}. The possibility that D-2 underwent a complete thermal cycling before recording on the DSC is minimal, due to its subambient M_s, with the lowest possible temperature experienced during the quench being 273 K. If a partial cycle were experienced this could explain smaller ordinate values for the first recorded cycle of D-2. An increase in subambient M_s temperatures by ordering of the parent phase structure due to room temperature aging has been demonstrated by Planes et al. [Ref. 8] and Dunne and Kennon [Ref. 4]. However the interval between homogenization and annealing was about two months longer for D-2 than D-1, so this explanation is not appropriate.

The initial (first 20 cycle) increase of M_{max} accompanied with a gradual decrease of A_{max} show the decrease of energy of transformation with cycling as previously demonstrated by Perkins and Muesing [Ref. 9], and in Kajiwara's [Ref. 10] research showing complete reproducibility was not obtained in Cu-Zn alloys until 20 cycles had been completed. With increasing number of cycles, M_{max} continues to rise until

75 cycles for D-1 and 30 cycles for D-2 at which time the M_{max} begins to decrease, contrary to research carried out by Li and Ansell [Ref. 11] showing a steady increase in M_s until approximately 300 cycles. After 35 cycles, the decrease in A_{max} with cycling lessens and the average A_{max} remains constant until about 80 cycles, and then continues to decrease. An examination of data points reveals a distinct sinusoidal pattern with frequency of about 15 thermal cycles and 1.25 K amplitude for both M_{max} and A_{max} curves. The accentuation of this pattern, which can not be attributed to experimental scatter, can be seen in Figure 4 where points that fall far below the curve are followed by points far above the curve. As the points represent the rate of energy absorption or evolution of the phase transformation, there appears to be a region in which the stability of the phase is contained, coupled with a cyclic pattern of energy release and storage. When a phase transformation occurs a definite quantity of energy is involved, represented on Figures 1 to 4 by the solid curve. If the maximum rate of energy transferral occurs at a lower than average temperature, representing increased stability of the original phase, there is energy storage within the structure available on the next cycle increasing the temperature of transformation and decreasing the stability of the original phase. The exact frequency and amplitude of the pattern is possibly determined by the degree of ordering and lattice structure of the alloy. These

properties, varying with minute changes in composition and heat treatment, could specify the numerical limits on the sinusoidal variance, with the characteristics of the sinusoid differing for dissimilar specimens.

B. TRANSMISSION ELECTRON MICROSCOPY

Sample groups D-1 and D-2 photographed at room temperature, approximately 30 K above A_f, were in the β parent phase range of stability. Any existing martensite plates are residual, surface or a result of stress inducement. For comparison of basic structure, Figure 5 taken of alloy F, M_s approximately 355 K, exhibits distinct, internally twinned, parallel martensite plates. The fine striations are a result of random faulting on the basal and twinning planes, as described for Cu-Al-Ni alloys by Tadaki [Ref. 12]. The sharp, linear interface is shown in Figure 6. All the remaining figures are of thermally cycled alloy D.

Figure 7 taken after one thermal cycle, shows the presence of vestigial ridges, a structure similar to that observed by other researchers. Schroeder and Wayman [Ref. 13] observed faint "ghosts" appearing, above M_s, on the surface of superelastically cycled Cu-Zn alloys. Kajiwara [Ref. 14] closely associated the ridges in Cu-Zn alloys, seen along directions parallel to those of martensite plate formation and increasing in number with increasing cycles, with the reproducible formation of martensite plates. Kajiwara also observed a similar structure in Fe-Ni alloys [Ref. 15] as

Figure 5. Alloy F showing internally twinned martensite plates. (40,000X)

Figure 6. Closeup of interface of Figure 5. (200,000X)

small islands elongated parallel to directions in which surface upheavals on the reverse transformation had formed, produced as a result of self stress-accommodation among reverse transforming plates. Tanner, Pelton, and Gronsky [Ref. 16] proposed that the ridges are due to fluctuations in the atomic order, concentrations or lattice strain. Observing Ni-Ti-Cu alloys in a TEM with a heating and cooling stage, Bricknell and Melton [Ref. 17] found that "ghost" martensite images associated with image mottling especially near the Bragg condition, ran parallel to martensite that had formed, and would reform in a burst manner. Figure 8 shows the remnants of self-accommodating martensite plates. The thin double needles perpendicular to the main plate appear to be strain-induced martensite similar to that described by Schroeder and Wayman for Cu-Zn alloys [Ref. 18], forming above M_s.

After five cycles, Figure 9 displays the numerous vestigial variants present including the fork-type morphology with nearly parallel shape strains, and spears with two variants forming pairwise bisected by a common symmetry plane, both described by Schroeder and Wayman [Ref. 18]. A variant evident here and in Figures 13, 28, and 30 is similar to the Type A butterfly martensite found in ferrous alloys, as described by Umemoto and Tamura [Ref. 19]. This type is composed of two plates with an irregular junction and smooth interface with the remaining parent phase; forming as a result of

Figure 7. Alloy D (1 thermal cycle). The light traces of vestigial ridges are evident. (27,000X)

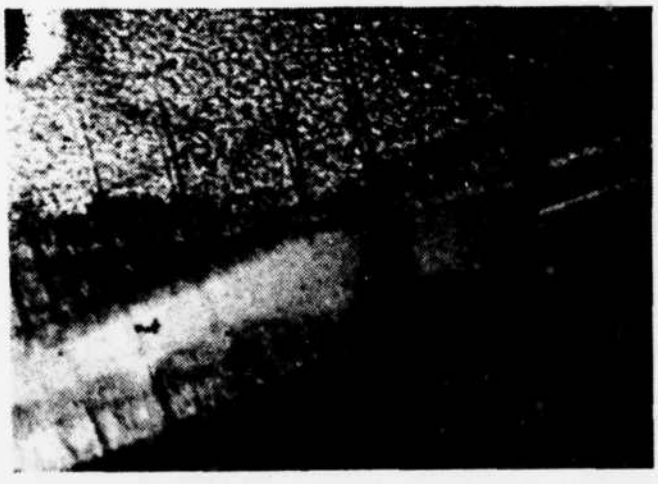

Figure 8. Alloy D (1 thermal cycle). Self-accommodating plates are seen with perpendicular needle-like stress-induced martensite. (14,000X)

imperfect self-accommodation due to the similarity of shape strain directions. The twins on the outer surface act as autocatylitic nucleation sites with the initially transformed plate generating slip which nucleates the second plate of the same variant. Figure 10 shows a closeup of a residual martensite plate with internally twinned and banded structure.

The intersection of three grains, shown in Figure 11 of a sample cycled ten times, displays the increase in number and variant forms of martensite. Two distinct grain boundary-vestige relationships are evident, with parallel bands terminating at the boundary in the two left grains as opposed to the cluttered arrangement of vestiges in the region of the boundary for the right grain. The formation of thermoelastic martensite is accompanied by shape changes that are restricted in part by grain constraint described by Dvorak and Hawbolt [Ref. 20]. When the matrix is constrained, as at the grain intersection, a higher energy is needed to produce the same amount of martensite. Parallel vestiges are again evident in the right hand side of Figure 11. Figure 12 shows the ridges becoming more distinct with increased cycling and a wave-like pattern resulting from the interaction of thermoelastic martensite formed in a continuous and thermoelastic manner. The increased definition of the vestigial ridges appear to aid in the cycling by enabling the parent phase to "anticipate" characteristics of the transition, as with increased development of the ridges M_{max} increases. An

Figure 9. Alloy D (5 thermal cycles). Numerous vestigial variants are displayed including fork, spear and butterfly morphologies. (10,000X)

Figure 10. Alloy D (5 thermal cycles). A residual martensite plate exhibits internally twinned and banded structure. (5,000X)

Figure 11. Alloy D (5 thermal cycles). The intersection of three grains reveals different vestige-grain boundary relationships. (5,000X)

Figure 12. Alloy D (5 thermal cycles). With increased cycling, the surface relief of ridges increases. (5,000X)

inertial-type barrier to transformation overcome by the formation of ridges may be responsible for the large change in M_{max} for the first few cycles.

Figure 13 exhibits two distinct martensite orientations in relation to a grain boundary. As discussed by Takezawa et al. [Ref. 21] the martensite transformation does not take place independently in the grains but proceeds with a strong interface across the boundary caused by the necessity for compatibility of the transformation strains at the boundary, resulting in the formation of α_1' martensite with its slip systems increasing the number of shear systems possible. As discussed by Perkins [Ref. 22] this effect decreases through the relaxation of stresses associated with grain boundary features by increased cycling. The spearlike martensite in the upper grain of Figure 13 is similar to that found in Cu-Al alloys by Villasenor, Huansota, and Maldonado [Ref. 23] of the twinned γ' type with $(121)\gamma'$ acting as the twinning plane. As exhibited by the closeup of the spears in Figure 14, the mottled, step-type structure of the vestigial spear-parent phase interface is quite different from the interfaces displayed by alloy F. The difference in orientation and relief of various vestigial plates is shown in Figure 15. An area with one distinct residual plate, exhibiting clearly the dissimilarity between vestigial ridges and residual plates is shown in Figure 16, with Figure 17 displaying the stress contours observed about this plate, indicative of the strain

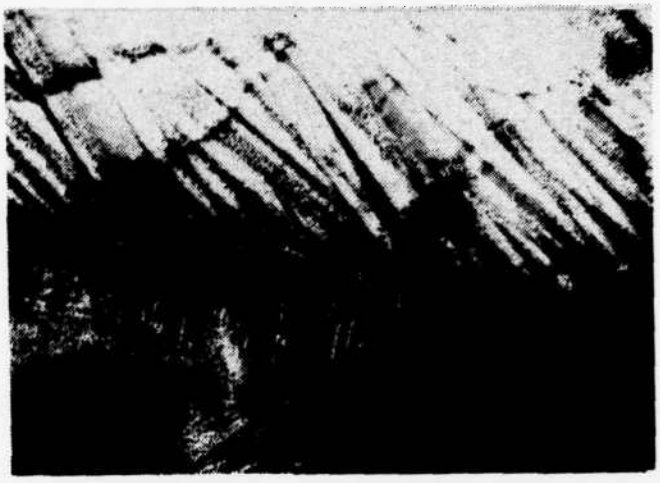

Figure 13. Alloy D (10 thermal cycles). Two distinct orientations of the vestigial ridges to the grain boundary are shown. (10,000X)

Figure 14. Alloy D (10 thermal cycles). A magnification of the spear structure of Figure 13 reveals a step-type structure. (27,000X)

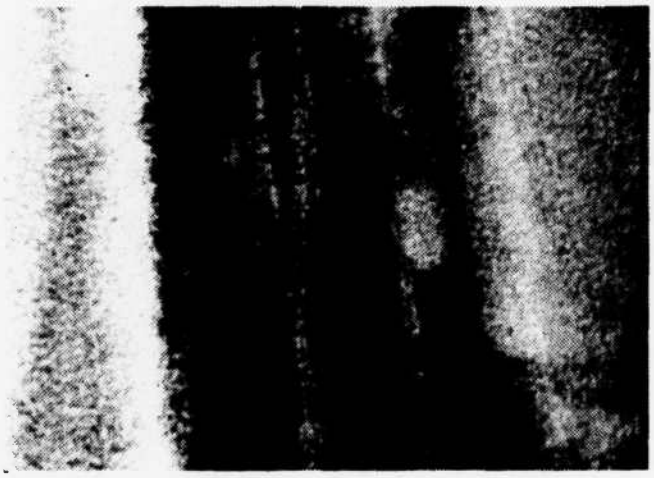

Figure 15. Alloy D (10 thermal cycles). Self-accommodating nature of plate structure is shown. (27,000X)

Figure 16. Alloy D (10 thermal cycles). An area with one residual plate is shown. (27,000X)

Figure 17. Alloy D (10 thermal cycles). A close-up of the plate of Figure 16. (100,000X)

field present. A similar residual plate in Figure 18, with interface shown in Figure 19, appears to have interior vestigial spears and band structures.

As the number of thermal cycles increases, so does the dislocation density, as revealed by Figures 20 and 21, with distinct angular relationships developed with the vestigial ridges which show increased surface relief. As discussed by Kajiwara [Ref. 10] and Beyer [Ref. 24], the increased density of dislocations with cycling is coupled to enhanced reversibility of transformation, with martensite formation preceded by dislocation rearrangement and new dislocations being generated with the reverse transformation. According to Jara et al. [Ref. 25] the dislocations found in the β phase of thermally cycled Cu-Zn-Al alloys have <111>β line directions and occur in rows in the <110>β direction, {110}β is considered as the slip plane containing pair-associated dislocations with type <100> Burgers vectors. The concept of growth accidents has been proposed as a mechanism of formation for these dislocations by Gleiter [Ref. 26] with interface movement generating dislocations in the lattice with distance increments dependent on the rate of migration of the boundary. The lowest resulting dislocation density will be in the region where the boundary just begins to migrate. Figure 22 shows three possible grains with a low-angle grain boundary possessing an unusual deviation from smoothness at the top of the figure. Some structure is definitely confined above the middle boundary,

Figure 18. Alloy D (10 thermal cycles). Another residual plate is bounded by a mottled matrix. (14,000X)

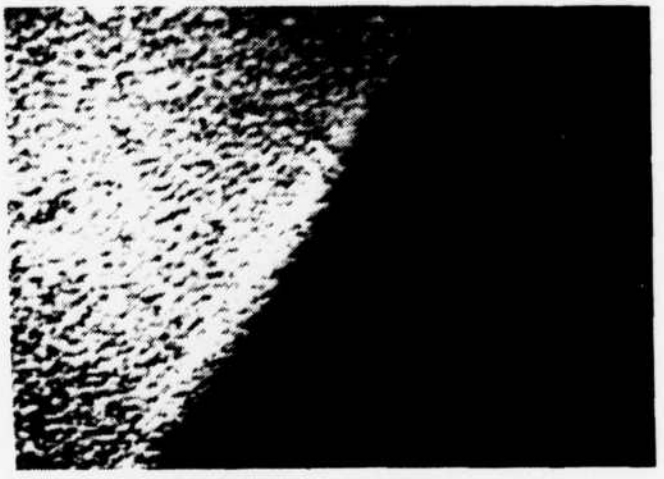

Figure 19. Alloy D (10 thermal cycles). A close-up view of the plate-matrix interface of Figure 18. (40,000X)

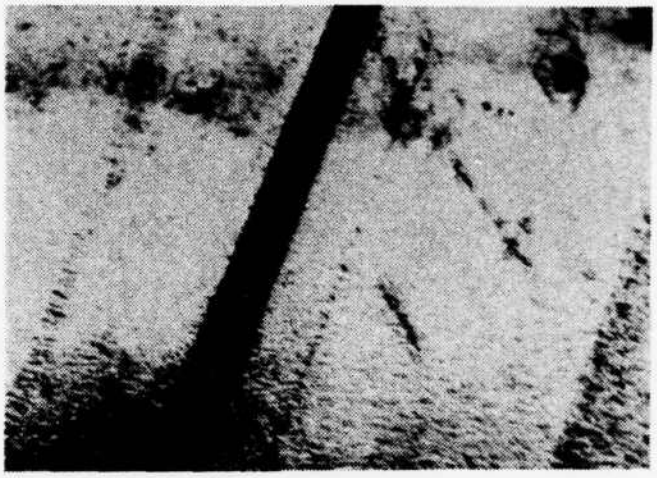

Figure 20. Alloy D (15 thermal cycles). Dislocations have a distinct angular relationship with vestigial structures. (20,000X)

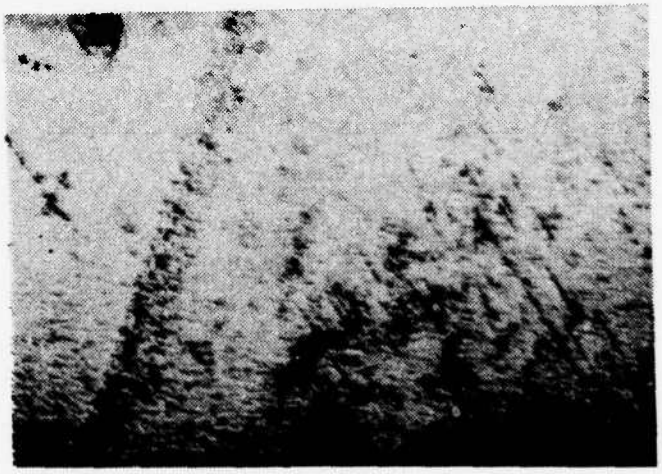

Figure 21. Alloy D (15 thermal cycles). A continuation of Figure 20 shows the concentration of dislocations to a distinct region of the matrix. (20,000X)

where on the right other structures continue across the boundary relatively undisturbed, although there appears to be some discontinuities at the boundary proper. None of the dislocation structures pass through the top boundary. In the left hand central grain, a very indistinct vestigial structure appears in an orientation perpendicular to the dislocations. The equi-distant and band-type segregation of dislocations is shown by the central region of Figure 23. Kajiwara's work with Cu-Zn alloys [Ref. 14] discusses banded dislocations with widths equal to widths of martensite plates. The Burgers vectors of dislocations were different for neighboring bands but the same for alternate bands, disallowing their origin as a result of release of accommodation strain around martensite plates during the bcc → 9R transformation. Therefore in the reverse transformation, the lattice invariant deformation must occur on different slip systems in the β phase for neighboring martensite plates with dislocations being introduced. The continued enhancement of surface relief of ridges and mottling effects with cycling is seen in Figure 24.

At a relatively low magnification a section with no major dislocation interaction is shown in Figure 25. The surface relief of the ridges can be related to a similar phenomena for Fe-Ni alloys discussed by Kajiwara [Ref. 27] with upheavals occurring along the habit plane and finer striations due to the detwinning of transformation twins. Upon examining the

Figure 22. Alloy D (15 thermal cycles). Dislocation structures are seen in relationship to two grain boundaries. (14,000X)

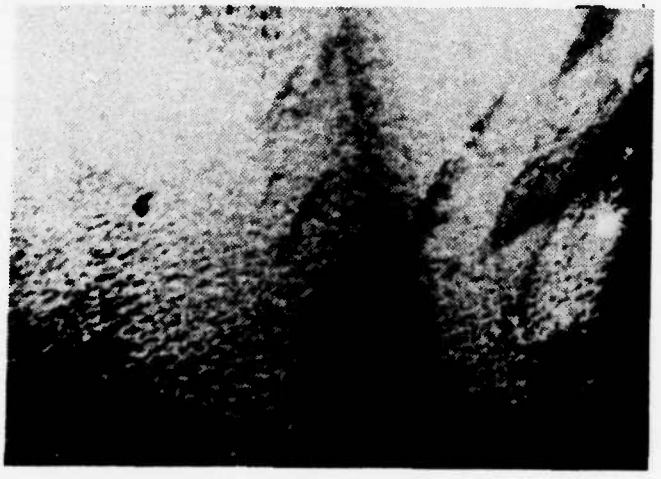

Figure 23. Alloy D (15 thermal cycles). The equidistant and band-type segregation of dislocations is displayed. (20,000X)

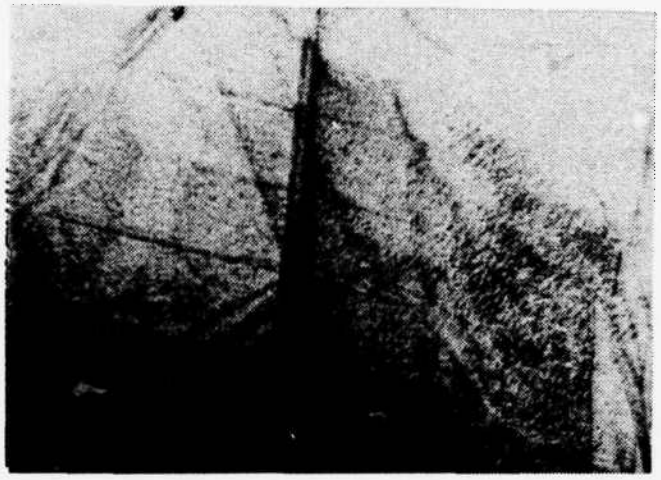

Figure 24. Alloy D (15 thermal cycles). As cycling continues, the surface relief of vestigial ridges continues to be enhanced. (14,000X)

ridges at 200,000X under dark-field technique, the distinct structure of a vestigial ridge is revealed in Figure 26 showing a stepped midrib bounded by parallel, twinned sides. It is possible that the ridges are primarily remnants of thermoelastic martensite which reverted by the burst mode, one of the two basic martensite growth and reversion modes described by Pops and Massalski [Ref. 28]. As the temperature is lowered below M_s, the initial slow growth of martensite needles was in the edge direction with others forming parallel, and a few nucleating and growing in other directions giving the characteristic V-shape regions. At a temperature M_B, lower than M_s, large quantities of martensite formed in bursts and disappeared with similar rapidity on heating. The general burst morphology consists of small Vs or parallelpipeds delineated by two variants of habit plane with the transformation producing lattice defects and plastic deformation, possibly serving as sites for subsequent martensitic transformation. Burst formation is associated with mechanical coupling between several habit plane variants that are nearly parallel to the plane on which initial martensite forms, with the presence of lattice strain reducing the amount of martensite occurring in a burst manner. Warlimont et al. [Ref. 29] suggest that the cessation in the formation of burst martensite occurs when the free enthalpy acting as the thermal component of the driving energy for martensitic plate growth drops below a critical value. As noted by Li and Ansell [Ref. 11] occurrence of burst martensite in Cu-Zn-Al

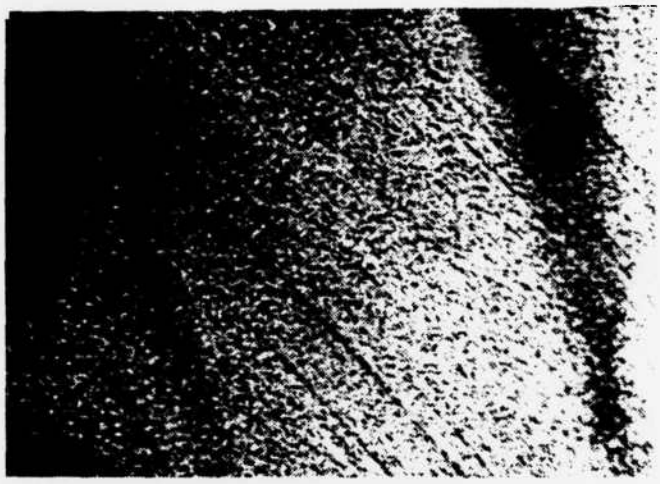

Figure 25. Alloy D (15 thermal cycles). Vestigial ridges are shown in a parallel arrangement. (14,000X)

Figure 26. Alloy D (15 thermal cycles). At higher magnification, a vestigial ridge of Figure 25 shows a distinct martensitic structure. (100,000X)

thermally cycled samples had ceased at sixty cycles, being replaced by continuously growing martensite. They observed the elongation rate of continuous growing martensite to be approximately 300 μ/min. The propagation of burst martensite at nearly sonic velocity, is about 10^8 orders of magnitude greater. The speed of propagation and remission appears too 'fast' for the atomic reshuffling to completely occur on the transition of martensite to parent phase and results in structured vestigial ridges, residual artifacts of the burst martensite. The increased mottling or tweed would be an alteration of the parent phase as a result of the reversion of continuously grown martensite. The formation of vestigial ridges serves to decrease the hysteresis of the transformation, increasing M_{max} by serving as nucleation sites, and decreasing A_{max} by acting as residual martensite structures. With the ridges' increase in relief or volume with cycling, there is a decrease in the amount of martensite reverting to the parent phase, and the average temperature at which the maximum rate of reversion occurs decreases. With about 50 cycles, as shown by Figures 1 to 4, the stabilization of M_{max} and A_{max} is associated with the cessation of burst martensite formation acting as an accommodation mechanism, as lattice strain becomes reduced by the introduction of dislocations and increase in varieties of martensite.

Figure 27 shows an interesting structure of a burst-type relief of a diamond-parallelpiped series interacting with

Figure 27. Alloy D (15 thermal cycles). Parallelpiped reliefs are possible vestigial structures of diamond-type martensite. (10,000X)

vestigial bands. The diamond morphology as described by Schroeder and Wayman [Ref. 18] contains four martensite variants twin-related in pair combinations with the parent. Relative to the parent phase, the long and short bisectors of the diamond are reflection planes. Saburi and Wayman [Ref. 30] have detailed through stereographic projection analysis how the diamond morphology can be derived from 18R(9R) or 2H structures.

As the number of cycles increase the interaction of vestigial forms as revealed by Figure 28, contributes to the decrease of M_s as pointed out by Oshima [Ref. 31] from the accumulation of internal stress resulting as a limit to the number of twins that can be introduced. The interaction of spear and wedge morphologies with the grain boundary is shown. A close-up revealing distinctive stepped structure, in Figure 29, shows a morphology similar to the γ'(2H) structure in Cu-Al-Ni-Fe-Mn alloys described by Hasan, Lorimer, and Ridley [Ref. 32], with internally twinned plates having no internal striations. In the range where β' type and γ' type martensite may be formed concurrently, small local changes in internal stresses are sufficient to transform the parent β phase into either of the two structures.

Figure 30 exhibits more of the butterfly martensite structure becoming more common and distinct because its formation is aided by the increased presence of dislocations resulting in constraint of the growth of martensite on one

Figure 28. Alloy D (100 thermal cycles). With increasing number of cycles, the interaction of vestigial forms is shown. (10,000X)

Figure 29. Alloy D (100 thermal cycles). On magnification of Figure 28, a γ-type structure is revealed. (27,000X)

side and nucleation on the other. As proposed by Kajiwara [Ref. 27], part of the driving force for the transformation reaction is supplied by residual internal stresses that have not been completely relieved by the formation of self-accommodating martensite variants. Therefore with morphologies such as butterfly forming as alternatives to self-accommodating martensite, there is less driving force and a lower M_s is evident than would be otherwise indicated. As cycling continues the intersection of groups of plates having different orientations are effective in reducing the growth of plates and stimulating the reversion as demonstrated by Yang, Laird, and Pope [Ref. 33]. This accounts for the decrease in A_{max} after about 70 cycles, as seen on Figures 3 and 4. The severe interaction of plates, with decrease in A_{max}, is exemplified by the double spear fork-within-a-fork morphology shown in Figure 31.

A sample cycled 77 times showed a distinct stacking fault structure shown in Figures 32 to 35, the width of the plate is 2.65 μm. Figure 32 shows a distinct band of lattice defects containing stacking faults, with remaining faults scattered throughout the plate in the remainder of the figure. Figure 33, a continuation of the plate in Figure 32, shows the angular relationships of the fault bands with the interface and internal structure of the martensite. Figure 34 shows the width of a group of stacking faults to be fairly uniform, measuring about 0.1 μm, with the accompanying

Figure 30. Alloy D (100 thermal cycles). With further cycling, the formation of butterfly martensite increases. (14,000X)

Figure 31. Alloy D (100 thermal cycles). The severe interaction of plates is revealed by the growth of a double spear within a fork. (14,000X)

Figure 32. Alloy D (77 thermal cycles). A distinct contour of lattice defects is contained in the plate. (20,000X)

Figure 33. Alloy D (77 thermal cycles). A continuation of Figure 32 exhibits banded and displaced stacking faults. (20,000X)

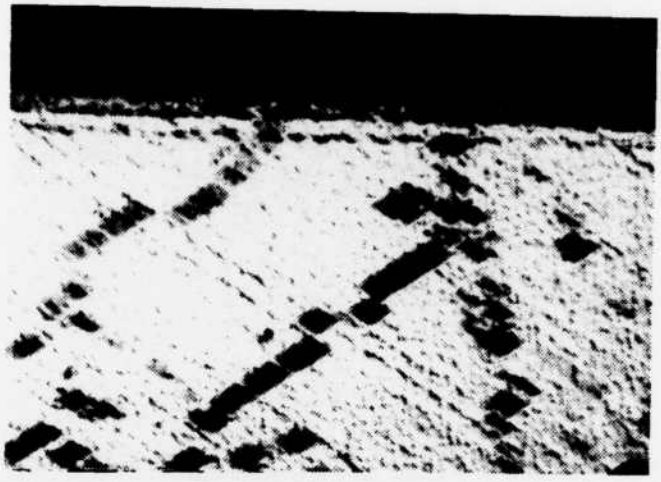

Figure 34. Alloy D (77 thermal cycles). The stacking faults of Figure 33 have been displaced by an internal twinning action of the martensite. (40,000X)

Figure 35. Alloy D (77 thermal cycles). The stacking faults contained in the contour of Figure 32 are displayed in magnitication. (200,000X)

structure of the martensite ridges having a spacing 25 nm to 75 nm. Although all groups of stacking faults are not displaced by the ridges, distinct movement has occurred. Figure 34 shows the stacking faults contained within the defect band of Figure 32, with the separation between fault centers measuring 10 nm. In Cu--18.5 at. % Zn--12.4 at. % Al, Andrade, Delaey, and Chandrasekaran [Ref. 34] noted similar structures with group widths varying from 1 μm to 0.1 μm. The faults were determined to be an $\{\bar{1}28\}$ type planes of β_1', different from the $(\bar{1}28)$ twinning planes separating specific self-accommodating variants. The $(\bar{1}\bar{2}8)$ and $(\bar{1}28)$ planes are both derived from {110} type β planes, but while $(\bar{1}28)$ is parallel to {110}β, $(\bar{1}28)$ is rotated 10°. The $(\bar{1}28)$ faults always terminate on other faults in the basal plane of the martensite. The variation in the density of stacking faults, as Ahlers [Ref. 35] points out, implies a concentration-dependent contribution to the free energy of the martensite as variations in the lattice parameter change the amount of secondary shear required to obtain an undistorted habit plane. The formation of stacking faults ending inside a plate, with movements of partial dislocations at the edges is described by Gotthardt [Ref. 36], and allows for accommodation of small changes in stress distribution. Where self-accommodating variatns exist there is a lower transformation strain and tendency for fault arrangement. The nonappearance of these faults in the majority

of samples is due to the dislocation structures in the martensite acting in a similar manner to the role of the partial dislocations existing at the edges of the stacking fault. The higher internal friction of martensite as compared to the matrix can be attributed to the movement of dislocations or stacking faults.

IV. CONCLUSIONS

1. Vestigial ridges, with a definite martensitic substructure, increase in number and relief up to about 50 cycles. Their formation is attributed to the incomplete reversion of burst martensite, with the cessation of burst formation occurring as lattice strain is reduced by the increase of dislocations, stacking faults, and varieties of martensite all acting as accommodation mechanisms.

2. The presence of butterfly morphology, stacking faults, dislocations, and burst martensite are indications of the imperfect self-accommodating nature of the martensite formed.

3. The variations of M_{max} and A_{max}, with cycling are attributable to a balance between numerous processes and constraints controlling the martensite transformation and reversion. The overall trends of M_{max} and A_{max} reflect the change of dominance with cycling of these processes and constraints.

4. Vestigial ridges, formed during martensite reversion, act as nucleation sites for subsequent martensite formation and prompt the initial increase in M_{max}. As the ridges continue to increase in number and relief, M_{max} continues to rise as the nucleation sites become more pronounced. Although ridge formation ceases after about 50 cycles, reflected by the leveling off of M_{max}, their establishment

as nucleation sites is shown by the continuation of higher values for M_{max}, then had occurred for the first few cycles.

5. The vestigial ridges decrease A_{max} by acting as residual martensite structures not transforming to the parent phase above A_f. As ridge relief increases, the quantity of martensite reverting to the parent phase decreases causing a decrease in A_{max}. With the cessation of ridge formation, A_{max} becomes a constant average value.

6. The necessity for compatibility of transformation strains at boundaries and interfaces places a requirement on the amount of energy required to produce a given amount of martensite. Further fluctuations in M_{max} are a result of the balance between the effect of increasing dislocation density (relieving transformation strains causing an increase in M_s), and group interactions (causing an accumulation of strains present and placing a limit on twins introduced decreasing M_s).

7. The decrease in A_{max} after about 70 cycles is attributed to continued plate interaction, reducing plate growth and stimulating reversion.

8. The variation of M_{max} and A_{max} for individual cycles follows a sinusoidal pattern, with a distinct frequency and amplitude that can be related to the lattices' capabilities for energy release and storage. The exact frequency and amplitude of the pattern is possibly determined by the degree of ordering and lattice structure of the alloy.

LIST OF REFERENCES

1. Olson, G.B., and Hartman, H., "Martensite and Life: Displacive Transformations as Biological Processes," Journal de Physique, Colloque C4, supplement au n° 12, Tome 43, p. 855, décembre 1982.

2. Perkins, J., "Shape Memory Behavior and Thermoelastic Martensitic Transformations," Materials Science and Engineering, v. 51, p. 182, 1981.

3. Delaey, L., Van Humbeek, J., Chandrasekaran, M., Janssen, J., Andrade, M. and Mwamba, N., "The Cu-Zn-Al Shape Memory Alloys," Metals Forum, v. 4, no. 3, pp. 164-174, 1981.

4. Dunne, D.P., and Kennon, N.F., "Ageing of Copper-Based Shape Memory Alloys," Metals Forum, v. 4, no. 3, pp. 176-183, 1981.

5. Sponholtz, R.O., An Investigation into the Two-Way Shape Memory Trainability of Polycrystalline Cu-Zn-Al Alloys, p. 17, M.S. Thesis, Naval Postgraduate School, Monterey, 1982.

6. International Copper Research Association, Inc., Report 78R1, Shape Memory Effect, Superelasticity and Damping in Copper-Zinc-Aluminum Alloys, by L. Delaey, A. Deruyttere, E. Aernoudt, and J.R. Roos, p. 50, 1 February 1978.

7. International Copper Research Association, Inc., Report 238, Shape Memory Effect and Internal Damping in Copper-Aluminum and Copper-Zinc Based Alloys, by L. Delaey, M. Chandrasekaran, W. De Jonghe, R. Rapacioli, and A. Deruytlere, p. 2, 30 April 1975.

8. Planes, A., Macqueron, J.L., Morin, M., and Guénin, G., "Calorimetric Study of Ordering in a β-Cu-Zn-Al Alloy," Materials Science and Engineering, v. 50, pp. 53-57, 1981.

9. Perkins, J. and Muesing, W.E., "Martensitic Transformation Cycling Effects in Cu-Zn-Al Shape Memory Alloys," Metallurgical Transactions A, v. 14A, pp. 33-36, January 1983.

10. Kajiwara, S., "Reproducibilities of Martensite Formation in Cyclic Transformation in Cu-Zn Alloys," Transactions of National Research Institute for Metals, vol. 18, no. 6, pp. 220-227, 1976.

11. Metallurgy Program, Office of Naval Research Technical Report 13, The Effect of Thermal Cycling on the Thermoelastic Martensitic Transformation in a Cu-Zn-Al Alloy, by J.C. Li and G.S. Ansell, pp. 2-9, December 1982.

12. Tadaki, T., Kakeshita, T., Shimizu, K., "Electron Microscope Study of the Matrix-Martensite Interface in Cu-Al-Ni Alloys," Journal de Physique, Colloque C3, supplément au n° 12, Tome 43, p. 855, décembre 1982.

13. Schroeder, T.A. and Wayman, C.M., "The Two Way Shape Memory Effect and other 'Training' Phenomena in Cu-Zn Single Crystals," Scripta Metallurgica, v. 11, pp. 225-230, 1977.

14. Kajiwara, S., "Reproducible Martensite Formation and Substructures Formed in the Parent Phase during Cyclic Transformation in Cu-Zn alloys," Proceedings of the First JIM International Symposium on "New Aspects of Martensitic Transformation," pp. 61-86, May 1976.

15. Kajiwara, S., "Reversibility of crystal orientation in the reverse martensitic transformation in Fe-Ni alloys," Philosophical Magazine A, v. 39, no. 3, pp. 325-334, 1979.

16. Tanner, L.E., Pelton, A.R., and Gronsky, R., "The Characterization of Pretransformation Morphologies: Periodic Strain Modulations," Journal de Physique, Colloque C4, supplément au n° 12, Tome 43, pp. 169-172, décembre 1982.

17. Bricknell, R.H. and Melton, K.N., "Thin Foil Electron Microscope Observations on NiTiCu Shape Memory Alloys," Metallurgical Transactions A v. 11A, pp. 1541-1546, September 1980.

18. Schroeder, T.A. and Wayman, C.M., "The Formation of Martensite and the Mechanism of the Shape Memory Effect in Single Crystals of Cu-Zn alloys," Acta Metallurgica, v. 25, pp. 1375-1391, 1977.

19. Umemoto, M. and Tamura, I., "The Morphology and Substructure of Butterfly Martensite in Ferrous Alloys," Journal de Physique, Colloque C4, supplément au n° 12, Tome 43, pp. 523-528, décembre 1982.

20. Dvorak, J. and Hawbolt, E.B., "Transformal Elasticity in a Polycrystalline Cu-Zn-Sn Alloy," Metallurgical Transactions, v. 6A, pp. 95-99, January 1975.

21. Takezawa, K., Izunmi, T., Chiba, H., and Sato, S., "Coherency of the Transformation Strain at the Grain Boundary and Fracture in Cu-Zn-Al Alloy," Journal de Physique, Colloque C4, supplément au n° 12, Tome 43, pp. 819-824, décembre 1982.

22. Perkins, J., "Rapid Solidification Effects in Martensitic Cu-Zn-Al Alloys," Metallurgical Transactions A, v. 13A, pp. 1367-1372, August 1982.

23. Villasenor, G.T., Huansota, A., and Maldonado, L., "Room Temperature Martensite Transformation of Cu--15.1% Al," Journal de Physique, Colloque C4, supplément au n° 12, Tome 43, pp. 621-622, décembre 1982.

24. Beyer, J., "Effect of Thermal Cycling on the Martensite Formation in Equiatomic TiNi," Journal de Physique, Colloque C4, supplément au n° 12, Tome 43, pp. 273-278, décembre 1982.

25. Jara, D.R., Morin, M., Esnouf, C., and Guénin, G., "Study of Dislocations in Cyclically Transformed β-phase in Cu-Zn-Al Alloys," Journal de Physique, Colloque C4, supplément au n° 12, Tome 43, pp. 735-740, décembre 1982.

26. Gleiter, H., Mahajan, S., and Bachman, K.J., "The Generation of Lattice Dislocations by Migrating Boundaries," Acta Metallurgica, v. 28, pp. 1603-1610, 1980.

27. Kajiwara, S., "Reversibility of shape deformation in the reverse martensitic transformation in Fe-Ni alloys," Philosophical Magazine A, v. 41, no. 3, pp. 403-415, 1980.

28. Pops, H., and Massalski, T.B., "Thermoelastic and Burst-Type Martensites in Copper-Zinc Beta-Phase Alloys," Transactions of the Metallurgical Society of AIME, v. 230, pp. 1662-1668, December 1964.

29. Warlimont, H., Delaey, L., Krishnan, V., Tas, H., "Review: Thermoelasticity, pseudoelasticity and the memory effects associated with martensite transformations. Part 3: Thermodynamics and kinetics," Journal of Material Science, v. 9, pp. 1543-1555, 1974.

30. Saburi, T., and Wayman, C.M., "Crystallographic Similarities in Shape Memory Martensites," Acta Metallurgica, v. 27, pp. 979-995, 1979.

31. Oshima, R., "Successive Martensitic Transformations in Fe-Pd Alloys," Scripta Metallurgica, v. 15, pp. 829-833, 1981.

32. Hasan, F., Lorimer, G.W., and Ridley, N., "Crystallography of Martensite in a Cu-10Al-5Ni-5Fe Alloy," Journal de Physique, Colloque C4, supplément au n° 12, Tome 43, pp. 653-658, décembre 1982.

33. Yang, N.Y.C., Laird, C., and Pope, D.P., "The Cyclic Stress-Strain Response of Polycrystalline, Pseudoelastic Cu-14.5 Wt Pct Al-3 Wt Pct Ni Alloy," Metallurgical Transactions A, v. 8A, pp. 955-962, June 1977.

34. Andrade, M., Delaey, L., and Chandrasekaran, M., "On Some Lesser Known Planar Defects in β_1' Cu-Zn-Al Martensite," Journal de Physique, Colloque C4, supplément au n° 12, Tome 43, pp. 673-678, décembre 1982.

35. Ahlers, M., "On the Stability of the Martensite in β-Cu-Zn alloys," Scripta Metallurgica, v. 8, pp. 213-215, 1974.

36. Gotthardt, P., "Stacking Fault Formation in a Faulted Cu-Zn-Al Martensite," Journal de Physique, Colloque C4, supplément au n° 12, Tome 43, pp. 667-671, décembre 1982.

INITIAL DISTRIBUTION LIST

		No. Copies
1.	Defense Technical Information Center Cameron Station Alexandria, Virginia 22314	2
2.	Library, Code 0142 Naval Postgraduate School Monterey, California 93940	2
3.	Department Chairman, Code 69 Department of Mechanical Engineering Naval Postgraduate School Monterey, California 93940	1
4.	Professor J. Perkins, Code 69Ps Department of Mechanical Engineering Naval Postgraduate School Monterey, California 93940	2
5.	LT Paul W. Bobowiec, USN c/o Mrs. Virginia Martin 188 Chesnut Avenue Cranston, Rhode Island 02910	3

DAT
FILM

shows the width of a group of stacking faults to be fairly uniform, measuring about 0.1 μm, with the accompanying

Figure 31. Alloy D (100 thermal cycles). The severe interaction of plates is revealed by the growth of a double spear within a fork. (14,000X)

of Figure 32 exhibits [illegible]
stacking faults. (20,000X)

Figure 32 are displayed in magnification.
(200,000X)

v. 27, pp. 973-999, 1979.

31. Oshima, R., "Successive Martensitic Transformations in Fe-Pd Alloys," Scripta Metallurgica, v. 15, pp. 829-833, 1981.

DTIC